Bioorganic Chemistry 86 (2019) 375–385

Contents lists available at ScienceDirect

Bioorganic Chemistry

journal homepage: www.elsevier.com/locate/bioorg

Discovery of novel chalcone-dithiocarbamates as ROS-mediated apoptosis inducers by inhibiting catalase

Dong-Jun Fu[a,b,d,1], Jia-Huan Li[b,1], Jia-Jia Yang[b,1], Ping Li[b], Yan-Bing Zhang[b], Simeng Liu[c], Zhong-Rui Li[b], Sai-Yang Zhang[a,b,*]

[a] School of Basic Medical Science, Zhengzhou University, Zhengzhou 450001, China
[b] School of Pharmaceutical Sciences & Collaborative Innovation Center of New Drug Research and Safety Evaluation, Zhengzhou University, Zhengzhou 450001, China
[c] Department of Gastroenterology, The Fifth Affiliated Hospital of Zhengzhou University, Zhengzhou 450052, China
[d] Department of Urology, University of California, Irvine, Orange, CA 92868, USA

ARTICLE INFO

Keywords:
Chalcone-dithiocarbamate
Catalase
DNA damage
Apoptosis
Epithelial-mesenchymal transition

ABSTRACT

Novel chalcone-dithiocarbamate hybrids were designed, synthesized and evaluated for antiproliferative activity against selected cancer cell lines (MGC803, MCF7, and PC3). Among these analogues, (*E*)-2-oxo-2-((4-(3-(3,4,5-trimethoxyphenyl)acryloyl)phenyl)amino)ethyl-4-(2-hydroxyethyl)piperazine-1-carbodithioate (**12d**) showed the best inhibitory activity against PC3 cells (IC_{50} = 1.05 μM). Cellular mechanism studies elucidated **12d** could inhibit colony formation, arrest cell cycle at G2/M phase and induce DNA damage against PC3 cells. Compound **12d** also induced mitochondrial apoptosis by caspase activation, MMP decrease, ROS production and catalase (CAT) inhibition. Importantly, **12d** inhibited epithelial-mesenchymal transition (EMT) process by regulating EMT-related proteins (E-cadherin, N-cadherin, Vimentin, MMP2, MMP9). These results indicated that **12d** is a promising lead compound and deserves further investigation for prevention and treatment of human prostate cancer.

1. Introduction

Chalcone derivatives have broad spectrum of biological activities including antimicrobial, anticancer, antiviral, antioxidant, anti-inflammatory, anticonvulsant, and antimalarial activities [1–3]. Especially, chalcones exhibited potent anticancer activity against cancer cells and the antitumor activity may be attributed to induction of apoptosis, blocking cell cycle progression, inhibition of angiogenesis and so on [4,5]. Chalcone analogue **1** (Fig. 1) displayed the potent antiproliferative activity against A549 cell lines with an IC_{50} value of 6.06 μM [6]. Chalcone **2** induced cell cycle blockage in G1 phase of cell cycle and inhibition of S phase in PC3 cells [7]. Chalcone **3** exhibited the inhibitory effect against MDA-MB-231 cells and HCT116 cells with IC_{50} values of 3.42 μM and 5.29 μM, respectively [8]. Chalcone **4** showed well cytotoxic activity against MCF7 and PC3 cell lines with IC_{50} values of 3.88 ± 1.03 μM and 3.15 ± 0.81 μM, respectively [9]. All these findings revealed that chalcone skeleton containing a 3,4,5-trimethoxyphenyl ring might be a potential antiproliferative fragment in anticancer drugs design.

Dithiocarbamates (DTCs) have received considerable attention due to their potent anticancer activity [10–12]. *Tert*-butyl 4-(((3-((3-(4-methoxyphenyl)-4-oxo-4*H*-chromen-7-yl)oxy)propyl)thio)carbonothioyl)piperazine-1-carboxylate **5** (Fig. 2) reported in our group displayed the potent inhibition of cell growth via MAPK signaling pathway and inhibit migration via Wnt pathway in PC3 cells [13]. Dual dithiocarbamate **6** showed the IC_{50} values of 54 nM and 23 nM against HepG2 and MCF7 cell lines, respectively [14]. (1,3-Benzodioxol-5-ylmethyl)-2-[4-(4-nitrophenyl)-1-piperazinylthiocarbamoylthio]acetamide **7** exhibited notable inhibitory effect on C6 cells with an IC_{50} value of 23.33 ± 7.63 μg/mL [15]. *N*-((2-methyl-4(3H)-quinazolinon-6-yl)methyl)dithiocarbamate **8** could arrested A549 cells at G2/M phase [16].

On the basis of these findings, in the present investigation we reported the synthesis and antiproliferative evaluation of a new series of chalcone-based dithiocarbamate derivatives as anticancer agents against selected cancer cell lines (MGC803, MCF7, and PC3) [17–22]. In this work, molecular hybridization strategy based on the incorporation of the chalcone and the dithiocarbamate into a single molecule has the potential to improve the antiproliferative efficacy. Importantly, the synthesized chalcone-dithiocarbamate hybrids were identified as ROS-mediated apoptosis inducers.

* Corresponding author at: School of Basic Medical Science, Zhengzhou University, Zhengzhou 450001, China.
E-mail address: saiyangz@zzu.edu.cn (S.-Y. Zhang).
[1] These authors contributed equally to this work.

https://doi.org/10.1016/j.bioorg.2019.01.023
Received 19 November 2018; Received in revised form 9 January 2019; Accepted 12 January 2019
Available online 16 January 2019
0045-2068/

2. Results and discussion

2.1. Chemistry

The synthetic routes towards chalcone analogues (**10a–10c** and **12a–12m**) were shown in Scheme 1. Commercially available **9** was reacted with acetophenone derivatives to form chalcones **10a–10c** by the Claisen-schmidt condensation, which was subjected to the acylation reaction to afford **11**. The target chalcone hybrids **12a–12m** were easily obtained with the mature reaction conditions developed by our group [23–25]. The purity of all biologically evaluated compounds was determined to be > 95% by reverse phase high performance liquid chromatography (HPLC) analysis.

2.2. Antiproliferative activity

In continuation with our efforts toward the identification of novel derivatives with anticancer potential [26], we evaluated the antiproliferative activity of chalcone analogues (**10a–10c** and **12a–12m**) against several cancer cell lines (MGC803, MCF7, and PC3) using the MTT assay. Due to potentially similar mode of action between reported dithiocarbamate derivatives and well-known 5-fluorouracil (5-FU), 5-Fu was used as the reference drug in the MTT assay [24].

From the antiproliferative results of compounds **10a–10c** in Table 1, chalcones without dithiocarbamate group displayed very weak activity against all cancer cell lines with IC_{50} values of > 40 μM. However, chalcone-dithiocarbamate hybrid **12a** showed moderate to potent

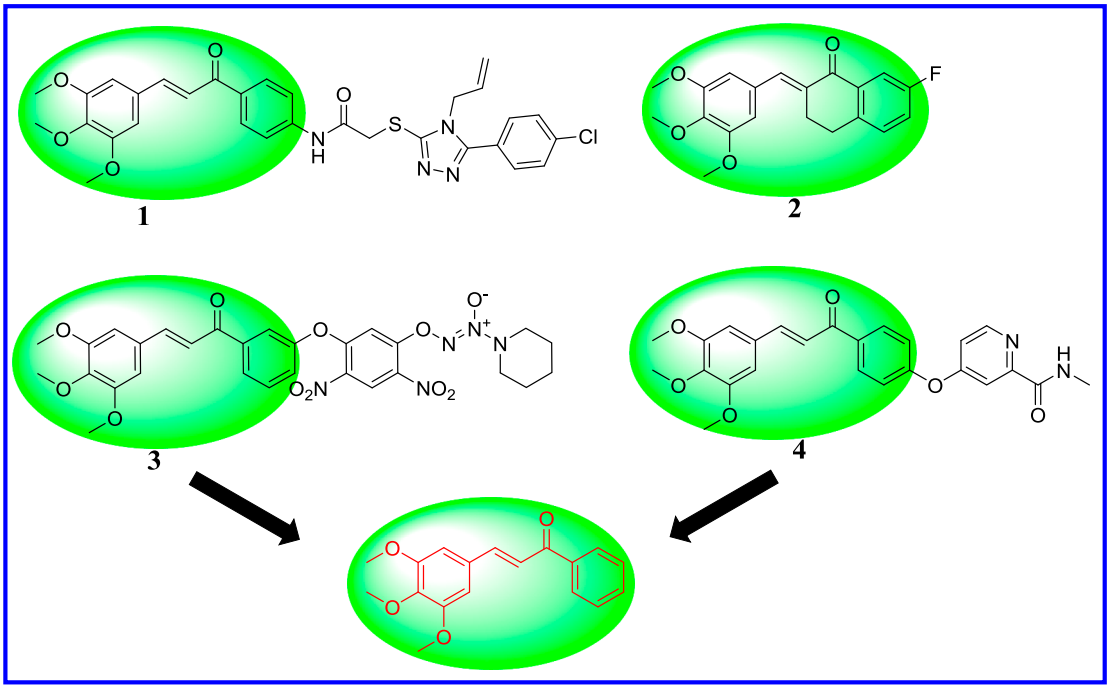

Fig. 1. Antitumor chalcone derivatives.

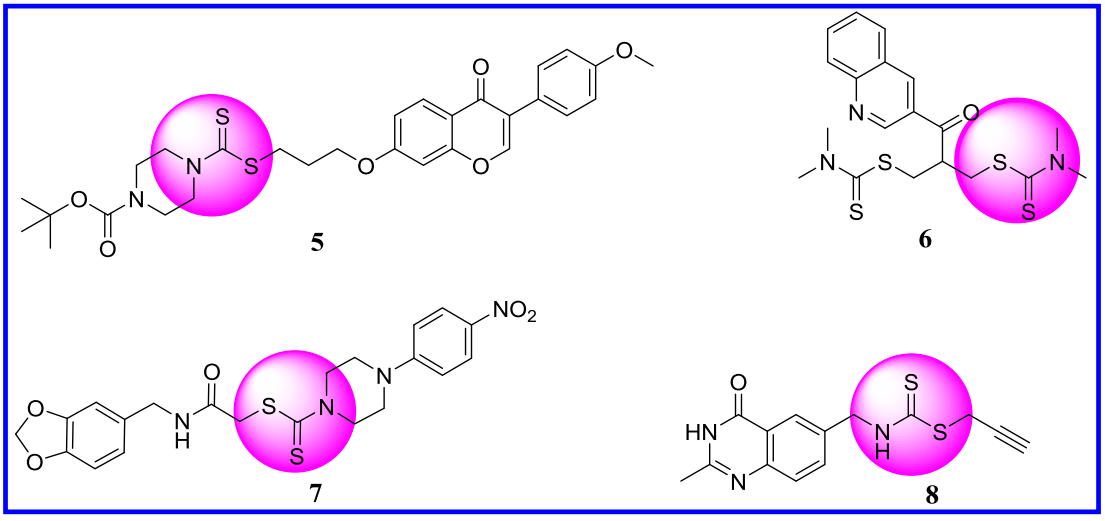

Fig. 2. Antitumor dithiocarbamate derivatives.

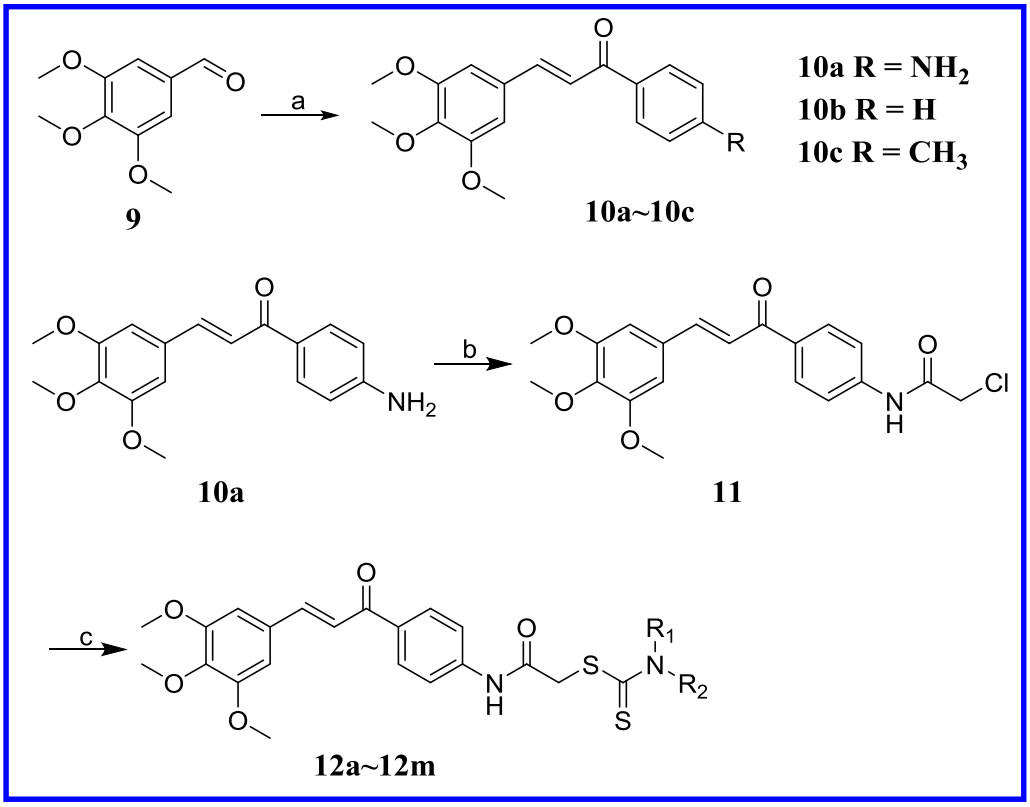

Scheme 1. Reagents and conditions: A: (a) acetophenone derivatives, NaOH, EtOH, reflux; (b) 2-chloroacetyl chloride, K_2CO_3, Acetone, reflux; (c) CS_2, substituted piperazine derivatives, $Na_3PO_4{\cdot}12H_2O$, acetone, rt.

Table 1
Antiproliferative activity of chalcones **10a–10c** and hybrid **12a**.

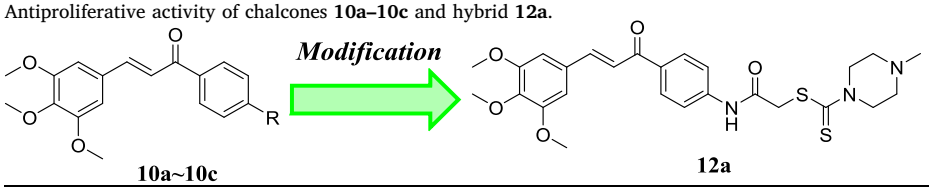

Compound	R	IC_{50} (μM)[a]		
		MGC803	PC3	MCF7
10a	NH_2	> 40	> 40	> 40
10b	H	> 40	> 40	> 40
10c	CH_3	> 40	> 40	> 40
12a	–	3.57 ± 0.08	2.40 ± 0.06	15.88 ± 1.10
5-FU	–	12.41 ± 0.94	29.31 ± 1.87	21.20 ± 3.60

[a] Antiproliferative activity was assayed by exposure for 72 h to substances and expressed as concentration required to inhibit tumor cell proliferation by 50% (IC_{50}). Data are presented as the means ± SDs from the dose-response curves of three independent experiments.

activity with IC_{50} values from 2.40 μM to 15.88 μM against all cancer cell lines. Based on this finding, it revealed that the dithiocarbamate group might exhibit an important role for the antiproliferative activity of chalcones.

In order to complete the structure activity relationships, a series of chalcone-dithiocarbamate hybrid were prepared and evaluated for their antiproliferative activity (MGC803, MCF7, and PC3). As shown in Table 2, chalcone-dithiocarbamate hybrid **12b–12i** exhibited the antiproliferative activity with IC_{50} values ranging from 1.05 to 37.25 μM. For these chalcone-dithiocarbamate hybrids **12b–12i**, the importance of substituents on the piperazine unit was also investigated in Table 2. Replacing the acetyl group (**12b**) by *t*-butyloxycarboryl group (**12e**) caused a decrease of activity. When the ethyl group attaching piperazine unit of compound **12c** was replaced by a hydroxyethyl group of compound **12d**, the antiproliferative activity was improved against MGC803 and PC3 cancer cell lines. In addition, chalcone-dithiocarbamate hybrids with 4-methoxy phenyl ring (**12f**) and pyrimidine ring (**12g**) attaching piperazine unit displayed weak activity against all cancer cell lines. All these modifications and structure activity relationship studies revealed that the substituents on the piperazine unit is important for their inhibitory activity.

To investigate the effect of piperazine unit, we also explored the antiproliferative activity of chalcone-dithiocarbamate hybrid **12j–12m** (Table 3). Compounds with morpholine (**12j**), thiomorpholine-1,1-dioxide (**12k**), piperidine (**12l**) and pyrrolidine (**12m**) were synthesized and evaluated for their antiproliferative activity against all these cell

Table 2
Antiproliferative activity of chalcone-dithiocarbamate hybrid **12b–12i**.

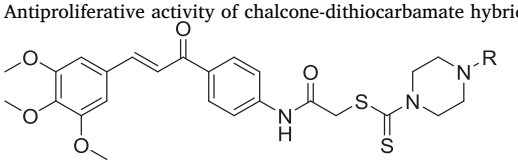

12b~12i

Compound	R	IC_{50}(μM)[a]		
		MGC803	PC3	MCF7
12b		2.48 ± 0.02	1.12 ± 0.02	12.25 ± 0.31
12c		1.99 ± 0.23	1.09 ± 0.04	17.70 ± 0.90
12d	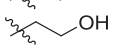	1.74 ± 0.16	1.05 ± 0.02	17.90 ± 1.70
12e		20.56 ± 0.18	15.60 ± 1.31	26.72 ± 1.23
12f	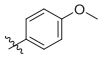	31.41 ± 1.42	27.08 ± 1.46	28.25 ± 0.87
12g		22.82 ± 0.78	27.25 ± 0.09	31.08 ± 0.59
12h	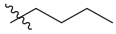	22.20 ± 0.64	17.34 ± 0.76	7.35 ± 1.14
12i		37.25 ± 0.14	4.19 ± 2.20	11.23 ± 0.33
5-FU	–	12.41 ± 0.94	29.31 ± 1.87	21.20 ± 3.60

[a] Antiproliferative activity was assayed by exposure for 72 h to substances and expressed as concentration required to inhibit tumor cell proliferation by 50% (IC_{50}). Data are presented as the means ± SDs from the dose-response curves of three independent experiments.

lines. Among them, compound **12j** with morpholine unit exhibited the most potent antiproliferative activity with an IC_{50} value of 1.28 μM against PC3 cells. We found that the *N*-heterocycle was important for the activity showing an over 12-fold activity loss, when the morpholine group (**12j**) was replaced with the pyrrolidine (**12m**).

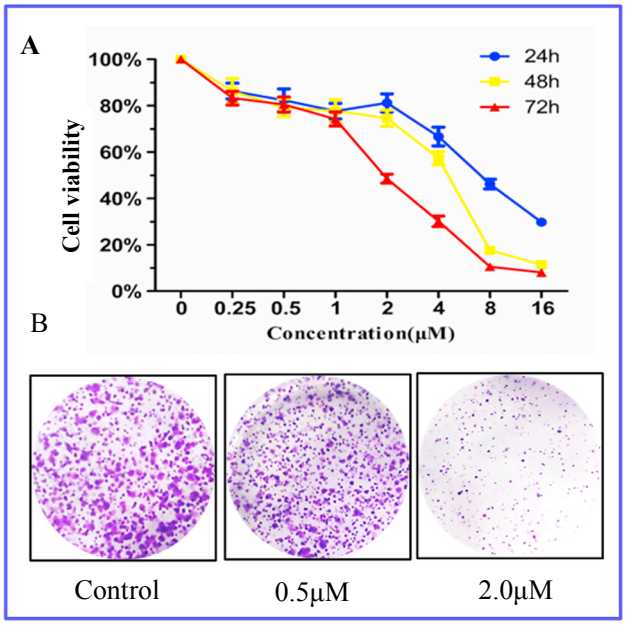

Fig. 3. (A) Cell viability of PC3 cell line with compound **12d** treatment; (B) Colony formation assay with **12d** (0.5 μM and 2 μM) at 10 days.

Table 3
Antiproliferative activity of chalcone-dithiocarbamate hybrid **12j–12m**.

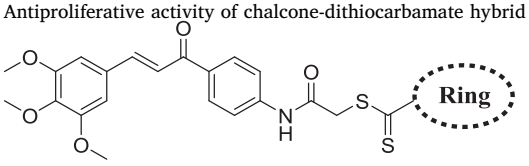

12j~12m

Compound	Ring	IC_{50}(μM)[a]		
		MGC803	PC3	MCF7
12j		8.71 ± 0.45	1.28 ± 0.08	9.52 ± 0.62
12k		11.21 ± 0.87	4.25 ± 0.47	3.98 ± 0.69
12l		5.36 ± 0.19	1.88 ± 0.07	17.25 ± 0.15
12m		11.24 ± 0.24	15.39 ± 0.34	18.25 ± 0.87
5-FU	–	12.41 ± 0.94	29.31 ± 1.87	21.20 ± 3.60

[a] Antiproliferative activity was assayed by exposure for 72 h to substances and expressed as concentration required to inhibit tumor cell proliferation by 50% (IC_{50}). Data are presented as the means ± SDs from the dose-response curves of three independent experiments.

2.3. *12d inhibits prostate cell proliferation and reduces colony formation*

Among all these targeted hybrids, compound **12d** showed the best anticancer activity in vitro with an IC_{50} value of 1.05 μM against PC3 cell lines. Thus, we selected **12d** to explore its detailed antiproliferative mechanisms against PC3 cells. PC3 cell line showed the obvious inhibition with the treatment of compound **12d** in time dependent and concentration dependent manners (Fig. 3A). We next studied the ability of PC3 cell line to form colonies on 6-well cell culture plates in the presence of compound **12d** (0.5 μM and 2 μM). The number of colonies was reduced in a concentration dependent manner, as shown in Fig. 3B. At the highest concentration of **12d** (2 μM), colony formation was reduced over 90% as compared to the untreated controls.

2.4. *12d arrests cell cycle at G2/M phase and regulates the expression of related proteins*

Cell cycle analysis of compound **12d** was done to detect cell distribution in each phase of cell cycle. From data obtained in (Fig. 4A and B), cell number at G2/M phase with the treatment of 5 μM **12d** changed to 67.36% compared with control, indicating compound **12d** could arrest cell cycle at G2/M phase against PC3 cell lines.

Cyclin-dependent kinases (CDKs) play a key role in the control of the G2/M transition of the cell cycle in prostate cancers [27]. To explore the effect of compound **12d** for cell cycle related proteins, the western blot assay was proceeded. As shown in Fig. 4C, compound **12d** upregulated the expression of P21 and decreased the expression of CDK1 and CyclinB1.

2.5. *12d inhibited epithelial-mesenchymal transition process*

The epithelial-mesenchymal transition (EMT) is a highly conserved cellular program that allows polarized, immotile epithelial cells to convert to motile mesenchymal cells [28]. Epithelial-mesenchymal transition could inhibit tubulin tyrosine ligase and promote microtubule stability, resulting in tubulin detyrosination and microtentacles formation for the attachment endothelial cell [29]. As shown in Fig. 5A, the purple part of pictures is the migrated cell, and the quantity of

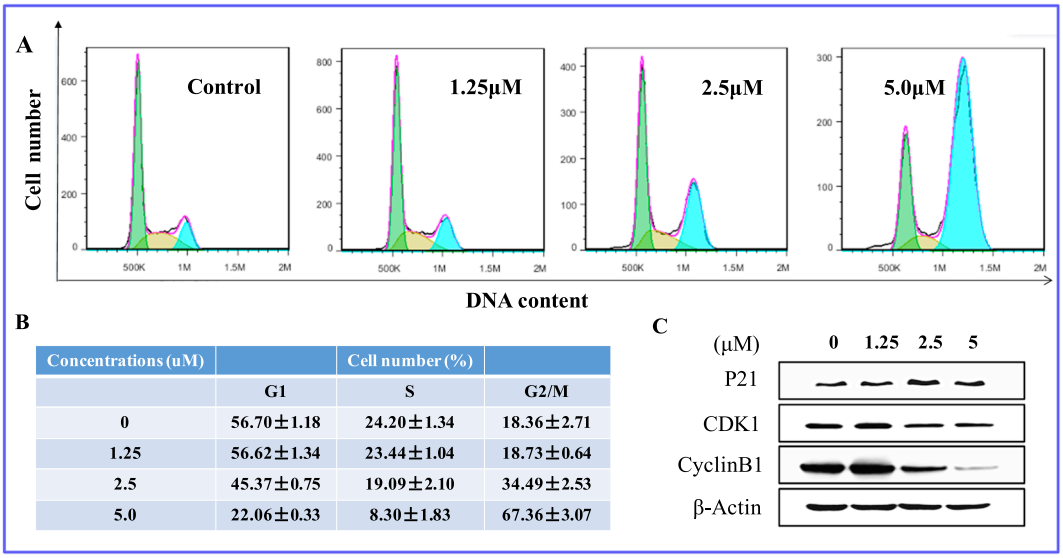

Concentrations (uM)		Cell number (%)	
	G1	S	G2/M
0	56.70±1.18	24.20±1.34	18.36±2.71
1.25	56.62±1.34	23.44±1.04	18.73±0.64
2.5	45.37±0.75	19.09±2.10	34.49±2.53
5.0	22.06±0.33	8.30±1.83	67.36±3.07

Fig. 4. (A) Cell cycle analysis of PC3 cells with treatment of **12d** (0, 1.25 μM, 2.5 μM and 5 μM) after 48 h treatment; (B) cell number of cycle phase; (C) the expression level of G2/M phase related proteins (P21, CDK1 and CyclinB1) after 48 h treatment.

migrated cells are decreased with the treatment of **12d**. The transwell results were also shown in Fig. 5B, the migration rate of migrated PC3 cells with the treatment of **12d** (control, 0.25 and 0.5 μM) were 100%, 50% and 31%, respectively. Then, we detected the expression level of epithelial-mesenchymal transition markers (E-cadherenin, N-cadherenin, MMP9, MMP2, and Vementin). From the results of Fig. 5C, **12d** could inhibit epithelial-mesenchymal transition process on PC3 cells by upregulation of E-cadherenin and downregulation of N-cadherenin, actived-MMP9, actived-MMP2, and Vementin.

2.6. *12d induced DNA damage*

DNA damage response constantly monitors DNA integrity and, in the presence of any type of DNA damage, activates transient cell cycle arrest and repair of DNA to ensure maintenance of genomic stability and cell viability [30,31]. Based on the blockage of cell cycle by compound **12d**, we assume that compound **12d** might induced DNA damage. The comet assay is a versatile and sensitive method for measuring single- and double-strand breaks in DNA [30]. To confirm

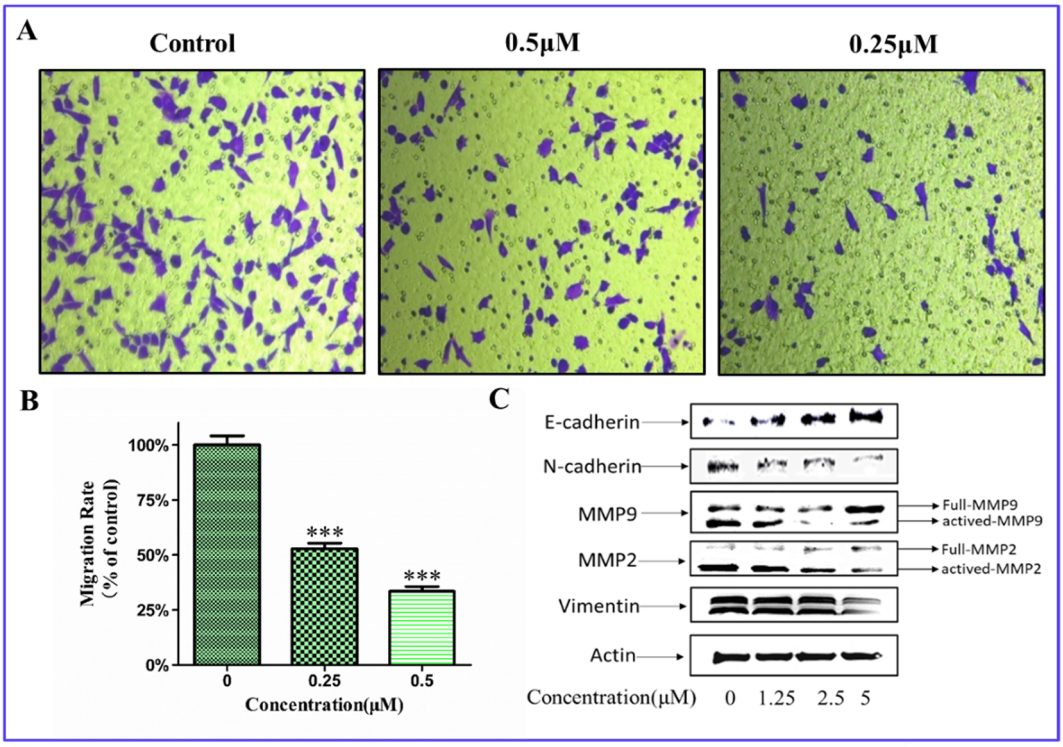

Fig. 5. (A) Transwell test of compound **12d** at 48 h on PC3 cells, the purple part of pictures is the migrated cell. (B) migration rate (%) of PC3 cells with the treatment of **12d** (0, 0.25 and 0.5 μM). (C) western blot analysis of EMT-related proteins at 48 h. ***$p < 0.001$ compared with the control.

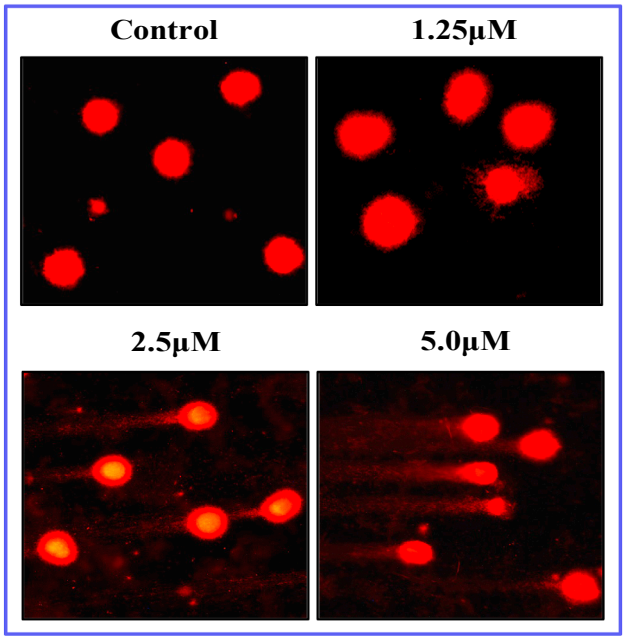

Fig. 6. Representative images of nuclei in the comet assay. PC3 cells were treated with compound **12d** at 48 h.

whether the potent compound **12d** generated the action to DNA, we quantified DNA damage by the comet assay in PC3 cells treated with **12d** at different concentrations (control, 1.25 μM, 2.5 μM and 5 μM). As shown in Fig. 6, the length of DNA tails was increased compared with control at a concentration dependent manner, indicating that compound **12d** displayed potent DNA-damaging ability.

2.7. *12d induced a decrease in the mitochondrial membrane potential.*

The loss of mitochondrial membrane potential (ΔΨm) displayed a key role during drug-induced apoptosis [31]. The maintenance of mitochondrial membrane potential (ΔΨm) is very important for bioenergetic function and mitochondrial integrity [32]. As shown in Fig. 7A, red fluorescence decreased with the increase of concentrations treatment and bright green fluorescence increased with the increase of concentrations, indicating that **12d** can induce a decrease in the mitochondrial membrane potential against PC3 cells. In addition, the percentage of cells at 5 μM was 20.9%, significantly higher than that of the control group (2.2%), also demonstrating that compound **12d** caused the mitochondrial membrane potential decrease in a concentration-dependent manner.

2.8. *12d induced apoptosis against PC3 cells*

In this work, the apoptotic analysis of **12d** against PC3 cells was performed with annexin V-FITC/PI double staining and quantitated by flow cytometry. From the results of Fig. 8A and B, the apoptotic population on PC3 cells increased to 27.9% (1.25 μM), 50.7% (2.5 μM), and 55.9% (5 μM), respectively, compared to control. All these datas indicated that compound **12d** could induce cell apoptosis against PC3 cell line.

Bcl-2 family proteins are important apoptosis regulators and overexpression of the prominent pro-survival Bcl-2 family members like Bcl-xl and Bcl-2 is a common feature responsible for deregulation of apoptosis in cancer cells [33]. We can see from the result in Fig. 8C that compound **12d** dramatically increased the level of Bad, and reduced the level of Bcl-2, Bid, and Bcl-xl. These results demonstrated that compound **12d** regulated Bcl-2 family proteins against PC3 cell line as a novel apoptosis inducer.

2.9. *12d induced the high ROS generation and inhibited the catalase (CAT) activity*

Reactive oxygen species (ROS) as regulators for cell apoptosis were appreciated to function as signaling molecules to affect cancer cells [34]. In this work, we tried to identify ROS effect in the course of **12d** induced-apoptosis. Therefore, the intracellular ROS generation in PC3 cells was marked by measuring the DCFH-DA fluorescence intensity. As shown in Fig. 9A and B, imaging analysis revealed that **12d** strongly generated ROS in PC3 cells in a concentration dependent manner.

Therefore, all these results suggested that compound **12d** could trigger the accumulation of intracellular ROS in PC3 cells.

Catalase (CAT) as an enzyme degrading hydrogen peroxide could be used as a therapeutic agent for cancer, but its successful application will depend on the distribution of the enzyme to the sites where ROS are generated [35]. Because **12d** generated high ROS accumulation, it was selected to explore the effect targeted to CAT enzyme. With the increase of concentrations, the activity of CAT was decreased (Fig. 9C). These results indicate that compound **12d** could induce the ROS level increase by inhibiting the activity of catalase.

2.10. *Molecular docking studies*

Molecular docking was performed to investigate binding modalities of the synthesized chalcone derivative **12d** and the catalase protein. In this paper, we choosed the PDB code: 1DGG based on the previous report [36]. As shown in Fig. 10, two carbonyl groups of **12d** formed two hydrogen bonds with the residues Tyr215 and Arg203. The nitrogen atom of amino formed a hydrogen bond with the residue Val450. Importantly, two sulphur atoms of the dithiocarbamate unit formed two hydrogen bonds with the residues Arg203 and Gln458, respectively, indicating the important role of dithiocarbamate for inhibitory activity against PC3 cells. In addition, the 3,4,5-trimethoxyphenyl ring of derivative **12d** formed hydrophobic interactions with the residues Pro304, Val450, Phe446 and Phe198.

3. Conclusion

We designed and synthesized of a series of novel chalcone-dithiocarbamate hybrids and evaluated their antiproliferative activity against cancer cell lines (MGC803, MCF7, and PC3). Among all these hybrids, **12d** showed the best inhibitory activity against PC3 cells with an IC_{50} of 1.05 μM. Preliminary biological mechanisms demonstrated that **12d** could reduce colony formation, induce DNA damage and arrest cell cycle at G2/M phase by the upregulation of P21 and downregulation of CDK1 and CyclinB1 in a concentration manner. By the scarification test and transwell test, **12d** inhibited the epithelial-mesenchymal transition process by adjusting the expression level of EMT related markers (E-cadherenin, N-cadherenin, MMP9, MMP2, and Vementin). Importantly, **12d** could cause PC3 cells apoptosis by inducing the mitochondrial membrane potential decrease and changing the expression level of BCl-2 family proteins. In addition, **12d** as a novel apoptosis inducer can also trigger the accumulation of intracellular ROS in PC3 cells by inhibiting the activity of catalase enzyme. In summary, compound **12d** could be a lead candidate for its further application in treatment of prostate cancer.

4. Experimental section

4.1. *General*

Commercial reagents and solvents were purchased from Sigma Aldrich and MedChemExpress. ^{13}C NMR and ^{1}H NMR spectra were recorded on a Bruker 100 MHz and 400 MHz spectrometer, respectively. High resolution mass spectra (HRMS) of all derivatives were recorded on a Waters Micromass Q-T of Micromass spectrometer by

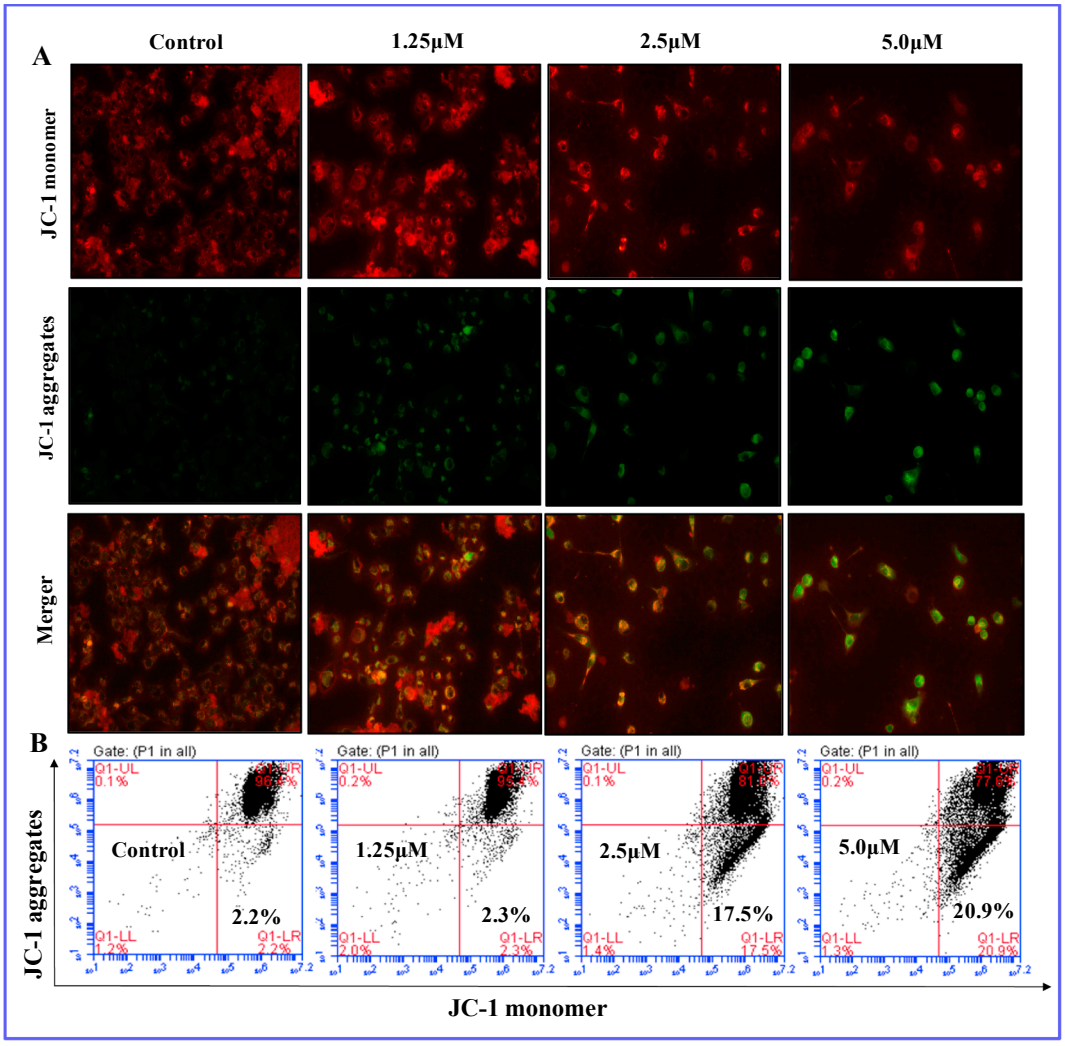

Fig. 7. (A) PC3 cells were treated with **12d** for 48 h. The samples were stained with JC-1 (magnification, 400×); (B) the treated samples were analyzed after JC-1 staining.

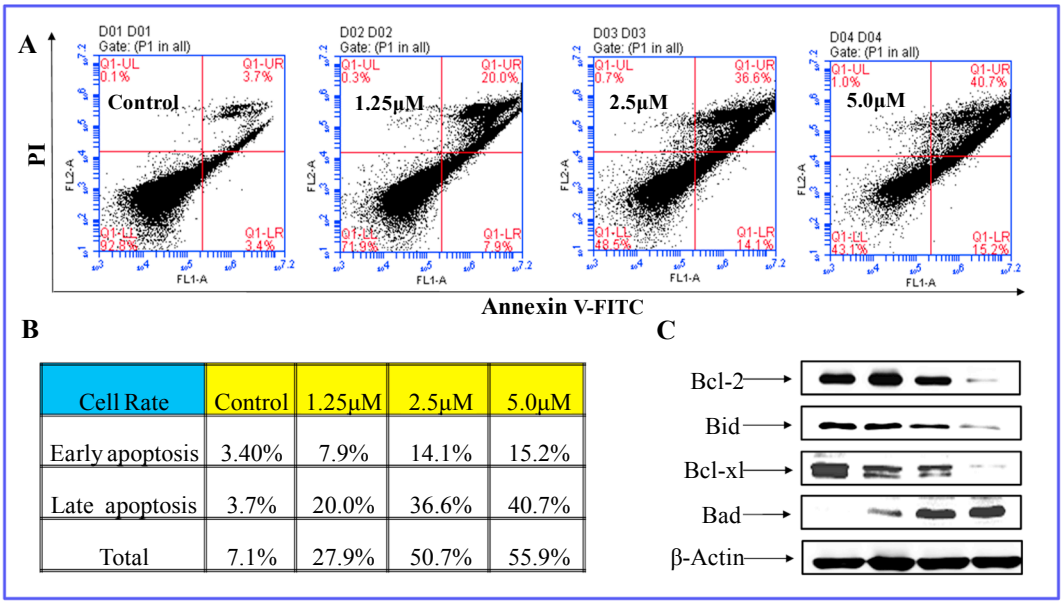

Cell Rate	Control	1.25μM	2.5μM	5.0μM
Early apoptosis	3.40%	7.9%	14.1%	15.2%
Late apoptosis	3.7%	20.0%	36.6%	40.7%
Total	7.1%	27.9%	50.7%	55.9%

Fig. 8. (A) The apoptosis analysis of **12d** treated cells after Annexin V-FITC/PI staining; (B) quantitative analysis of cell apoptosis; (C) western blot analysis of apoptosis-related proteins at 48 h.

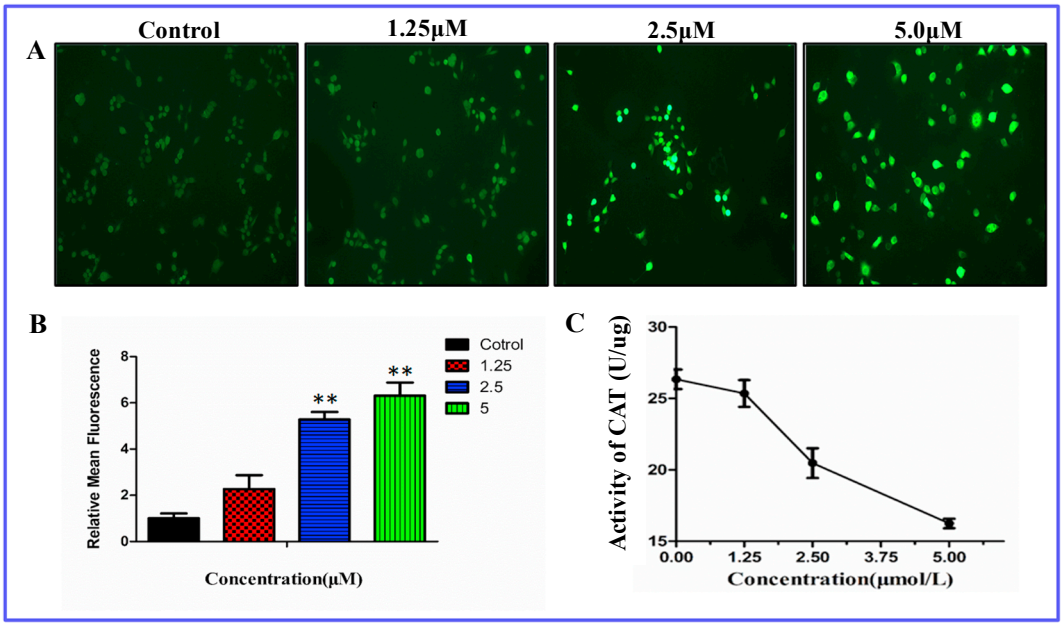

Fig. 9. (A) PC3 cells were stained by DCFH-DA after 24 h treatment to detect intracellular ROS level; (B) quantitative analysis of fluorescence; (C) effect of **12d** on inhibiting CAT activity. $^{**}p < 0.01$ compared with the control.

electrospray ionization (ESI). The purity of all biologically evaluated compounds was determined to be > 95% by reverse phase high performance liquid chromatography (HPLC) analysis.

*4.2. General procedure for the synthesis of compound **11***

To a solution of (*E*)-1-(4-aminophenyl)-3-(3,4,5-trimethoxyphenyl) prop-2-en-1-one **10a** (0.5 mmol, 1.0 eq) in acetone (5 mL) was added K_2CO_3 (0.75 mmol, 1.5 eq) at reflux condition, and then the 2-chloroacetyl chloride (0.75 mmol, 1.5 eq) was added dropwise. Upon completion, EtOAc and H_2O were added. The organic layers were washed with H_2O for three times, and then washed with brine, dried over $MgSO_4$ and evaporated to give the products. The residue was purified with column chromatography (hexane: EtOAc = 8:1) to obtain analogue ***11***.

*4.3 General procedure for the synthesis of compounds **12a–12l***

(*E*)-2-chloro-N-(4-(3-(3,4,5-trimethoxyphenyl)acryloyl)phenyl)acetamide (0.1 g, 1 eq), CS2 (2 eq), secondary amine (1 eq) and $Na_3PO_4{\cdot}12H_2O$ (0.5 eq) were added in acetone (5 mL). The mixture was stirred at room temperature for 6 h. Upon completion, the solvent was removed under reduced pressure, the residue was extracted with dichloromethane, washed with water, brine, dried with anhydrous Na_2SO_4 and concentrated under reduced pressure. The residue was purified with column chromatography (hexane: EtOAc = 10:1) to obtain analogue **12a–12l**.

4.3.1. (E)-2-chloro-N-(4-(3-(3,4,5-trimethoxyphenyl)acryloyl)phenyl) acetamide (11)

Yellow solid; M.p.: 179–180 °C; Yield: 30%. ^{1}H NMR (400 MHz, DMSO-d_6) δ 10.68 (s, 1H), 8.20 (d, J = 8.7 Hz, 2H), 7.90 (d, J = 15.5 Hz, 1H), 7.81 (d, J = 8.7 Hz, 2H), 7.69 (d, J = 15.5 Hz, 1H), 7.24 (s, 2H), 4.33 (s, 2H), 3.87 (s, 6H), 3.72 (s, 3H). ^{13}C NMR (100 MHz, DMSO-d_6) δ 187.97, 165.70, 153.58, 144.51, 143.29, 140.15, 133.39, 130.77, 130.43, 121.53, 119.19, 106.96, 60.61, 56.60, 44.11. HR-MS (ESI):Calcd. $C_{20}H_{21}ClNO_5$, $[M+H]^+$ m/z: 390.1108, found: 390.1112.

4.3.2. (E)-2-oxo-2-((4-(3-(3,4,5-trimethoxyphenyl)acryloyl)phenyl) amino)ethyl 4-methylpiperazine-1-carbodithioate (12a)

Yellow solid; M.p.: 176–177 °C; Yield: 28%. ^{1}H NMR (400 MHz,

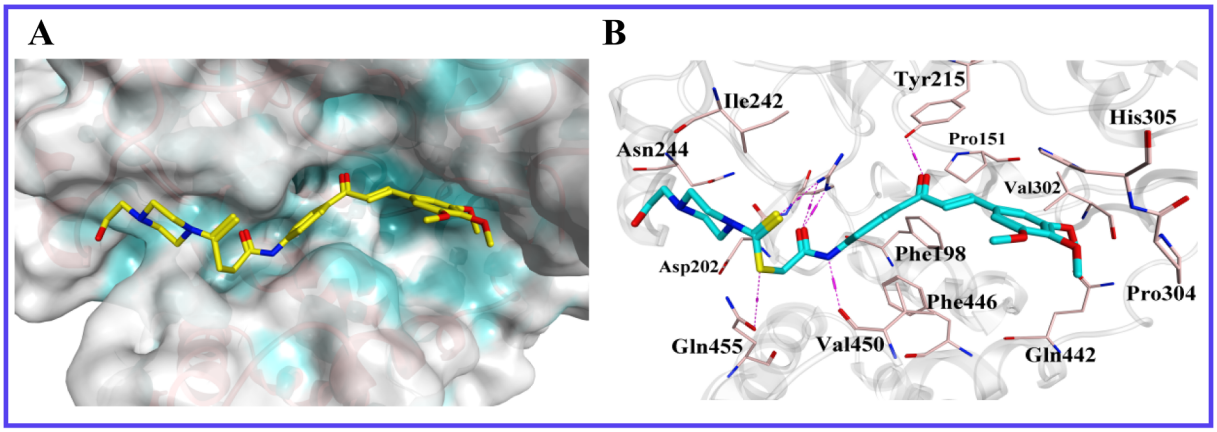

Fig. 10. (A) Protein surface map was used to show the binding of **12d** and CAT, where, blue is the hydrophobic surface of CAT, yellow is the **12d**.; (B) low-energy binding conformation of **12d** bound to CAT. **12d** (green), hydrogen bonds (purple) and protein residues (pink) were as shown.

DMSO-d_6) δ 10.70 (s, 1H), 8.18 (d, J = 8.7 Hz, 2H), 7.90 (d, J = 15.5 Hz, 1H), 7.80 (d, J = 8.7 Hz, 2H), 7.69 (d, J = 15.5 Hz, 1H), 7.23 (s, 2H), 4.33 (s, 2H), 4.20 (d, J = 9.2 Hz, 2H), 3.96 (s, 2H), 3.87 (s, 6H), 3.72 (s, 3H), 2.42 (s, 4H), 2.22 (s, 3H). ^{13}C NMR (100 MHz, DMSO-d_6) δ 194.42, 187.40, 165.98, 153.07, 143.89, 143.35, 139.61, 132.44, 130.30, 129.92, 121.06, 118.35, 106.43, 60.10, 56.10, 53.87, 44.96, 41.31, 40.11. HR-MS (ESI):Calcd. $C_{26}H_{32}N_3O_5S_2$, $[M+H]^+$ m/z: 530.1783, found: 530.1787.

4.3.3. (E)-2-oxo-2-((4-(3-(3,4,5-trimethoxyphenyl)acryloyl)phenyl) amino)ethyl 4-acetylpiperazine-1-carbodithioate (12b)

Yellow solid; M.p.: 207–208 °C; Yield: 27%. ^{1}H NMR (400 MHz, DMSO-d_6) δ 10.71 (s, 1H), 8.19 (d, J = 8.7 Hz, 2H), 7.90 (d, J = 15.5 Hz, 1H), 7.80 (d, J = 8.7 Hz, 2H), 7.69 (d, J = 15.5 Hz, 1H), 7.23 (s, 2H), 4.35 (s, 2H), 4.32–4.17 (m, 2H), 4.02 (dd, J = 13.7, 6.5 Hz, 2H), 3.87 (s, 6H), 3.72 (s, 3H), 3.63 (d, J = 7.0 Hz, 4H), 2.04 (s, 3H). ^{13}C NMR (100 MHz, DMSO-d_6) δ 194.81, 187.41, 168.67, 165.92, 153.07, 143.90, 143.32, 139.61, 132.46, 130.30, 129.93, 121.05, 118.36, 106.43, 60.10, 56.10, 44.40, 41.26, 30.65, 21.20. HR-MS (ESI):Calcd. $C_{27}H_{32}N_3O_6S_2$, $[M+H]^+$ m/z: 558.1733, found: 558.1737.

4.3.4. (E)-2-oxo-2-((4-(3-(3,4,5-trimethoxyphenyl)acryloyl)phenyl) amino)ethyl 4-ethylpiperazine-1-carbodithioate (12c)

Yellow solid; M.p.: 162–163 °C; Yield: 36%. ^{1}H NMR (400 MHz, DMSO-d_6) δ 10.69 (s, 1H), 8.18 (d, J = 8.7 Hz, 2H), 7.90 (d, J = 15.5 Hz, 1H), 7.80 (d, J = 8.6 Hz, 2H), 7.69 (d, J = 15.5 Hz, 1H), 7.23 (s, 2H), 4.32 (s, 2H), 4.21 (s, 2H), 3.95 (s, 2H), 3.87 (s, 6H), 3.72 (s, 3H), 2.46 (s, 4H), 2.37 (q, J = 7.1 Hz, 2H), 1.02 (t, J = 7.1 Hz, 3H). ^{13}C NMR (100 MHz, DMSO-d_6) δ 194.22, 187.40, 166.00, 153.07, 143.90, 143.34, 139.61, 132.44, 130.30, 129.92, 121.05, 118.35, 106.43, 60.10, 56.10, 55.81, 51.67, 50.99, 41.27, 11.82. HR-MS (ESI):Calcd. $C_{27}H_{34}N_3O_5S_2$, $[M+H]^+$ m/z: 544.1940, found: 544.1948.

4.3.5. (E)-2-oxo-2-((4-(3-(3,4,5-trimethoxyphenyl)acryloyl)phenyl) amino)ethyl-4-(2-hydroxyethyl)piperazine-1-carbodithioate (12d)

Yellow solid; M.p.: 168–169 °C; Yield: 38%. ^{1}H NMR (400 MHz, DMSO-d_6) δ 10.67 (s, 1H), 8.18 (d, J = 8.8 Hz, 2H), 7.90 (d, J = 15.5 Hz, 1H), 7.80 (d, J = 8.8 Hz, 2H), 7.69 (d, J = 15.5 Hz, 1H), 7.23 (s, 2H), 4.49 (t, J = 5.2 Hz, 1H), 4.33 (s, 2H), 4.21 (s, 2H), 3.95 (s, 2H), 3.87 (s, 6H), 3.72 (s, 3H), 3.53 (q, J = 5.7 Hz, 2H), 2.54 (s, 4H), 2.45 (t, J = 6.0 Hz, 2H). ^{13}C NMR (100 MHz, DMSO-d_6) δ 194.67, 187.91, 166.51, 153.58, 144.40, 143.84, 140.12, 132.95, 130.80, 130.43, 121.56, 118.86, 106.94, 60.61, 59.94, 58.94, 56.60, 56.32, 52.96, 41.69. HR-MS (ESI):Calcd. $C_{27}H_{34}N_3O_6S_2$, $[M+H]^+$ m/z: 560.1889, found: 560.1893.

4.3.6. Tert-butyl-(E)-4-(((2-oxo-2-((4-(3-(3,4,5-trimethoxyphenyl) acryloyl)phenyl)amino)ethyl)thio)carbonothioyl)piperazine-1-carboxylate (12e)

Yellow solid; M.p.: 207–209 °C; Yield: 56%. ^{1}H NMR (400 MHz, DMSO-d_6) δ 10.69 (s, 1H), 8.18 (d, J = 8.8 Hz, 2H), 7.90 (d, J = 15.5 Hz, 1H), 7.79 (d, J = 8.8 Hz, 2H), 7.68 (d, J = 15.5 Hz, 1H), 7.23 (s, 2H), 4.32 (d, J = 14.3 Hz, 2H), 4.22 (s, 2H), 4.03 (dd, J = 12.6, 5.5 Hz, 2H), 3.87 (s, 6H), 3.72 (s, 3H), 3.49 (s, 4H), 1.43 (s, 9H). ^{13}C NMR (100 MHz, DMSO-d_6) δ 194.83, 187.42, 165.93, 153.67, 153.07, 143.90, 143.32, 139.61, 132.45, 130.29, 129.92, 121.05, 118.36, 106.43, 79.40, 60.11, 56.10, 41.26, 27.99. HR-MS (ESI):Calcd. $C_{30}H_{38}N_3O_7S_2$, $[M+H]^+$ m/z: 616.2151, found: 616.2155.

4.3.7. (E)-2-oxo-2-((4-(3-(3,4,5-trimethoxyphenyl)acryloyl)phenyl) amino)ethyl- 4-(4-methoxyphenyl)piperazine-1-carbodithioate (12f)

Yellow solid; M.p.: 150–152 °C; Yield: 74%. ^{1}H NMR (400 MHz, DMSO-d_6) δ 10.70 (s, 1H), 8.18 (d, J = 8.8 Hz, 2H), 7.90 (d, J = 15.5 Hz, 1H), 7.80 (d, J = 8.8 Hz, 2H), 7.69 (d, J = 15.5 Hz, 1H), 7.23 (s, 2H), 6.94 (d, J = 9.1 Hz, 2H), 6.85 (d, J = 9.1 Hz, 2H), 4.35 (s, 4H), 4.12 (s, 2H), 3.87 (s, 6H), 3.71 (d, J = 9.8 Hz, 6H), 3.16 (s, 4H). ^{13}C NMR (100 MHz, DMSO-d_6) δ 194.47, 187.42, 165.98, 153.39, 153.08, 144.37, 143.91, 143.34, 139.61, 132.45, 130.30, 129.93, 121.06, 118.37, 117.89, 114.33, 106.43, 60.11, 56.11, 55.16, 49.33, 41.28. HR-MS (ESI):Calcd. $C_{32}H_{36}N_3O_6S_2$, $[M+H]^+$ m/z: 622.2046, found: 622.2049.

4.3.8. (E)-2-oxo-2-((4-(3-(3,4,5-trimethoxyphenyl)acryloyl)phenyl) amino)ethyl −4-(pyrimidin-2-yl)piperazine-1-carbodithioate (12g)

Yellow solid; M.p.: 176–178 °C; Yield: 80%. ^{1}H NMR (400 MHz, DMSO-d_6) δ 10.71 (s, 1H), 8.42 (s, 1H), 8.41 (s, 1H), 8.18 (d, J = 8.8 Hz, 2H), 7.90 (d, J = 15.5 Hz, 1H), 7.81 (d, J = 8.8 Hz, 2H), 7.69 (d, J = 15.5 Hz, 1H), 7.23 (s, 2H), 6.70 (s, 1H), 4.51 (s, 2H), 4.37 (s, 2H), 4.11 (s, 2H), 3.90 (s, 4H), 3.87 (s, 6H), 3.72 (s, 3H). ^{13}C NMR (100 MHz, DMSO-d_6) δ 210.20, 194.64, 187.41, 165.96, 160.80, 157.98, 153.08, 143.89, 143.33, 139.63, 132.46, 130.30, 129.92, 121.06, 118.37, 110.62, 106.44, 68.66, 60.11, 56.62, 56.11, 42.46. HR-MS (ESI):Calcd. $C_{29}H_{32}N_5O_5S_2$, $[M+H]^+$ m/z: 594.1845, found: 594.1849.

4.3.9. (E)-2-oxo-2-((4-(3-(3,4,5-trimethoxyphenyl)acryloyl)phenyl) amino)ethyl −4-butylpiperazine-1-carbodithioate (12h)

Yellow solid; M.p.: 130–132 °C; Yield: 82%. ^{1}H NMR (400 MHz, DMSO-d_6) δ 10.69 (s, 1H), 8.19 (d, J = 8.8 Hz, 2H), 7.91 (d, J = 15.5 Hz, 1H), 7.81 (d, J = 8.8 Hz, 2H), 7.70 (d, J = 15.5 Hz, 1H), 7.24 (s, 2H), 4.33 (s, 2H), 4.21 (s, 2H), 3.95 (s, 2H), 3.88 (s, 6H), 3.73 (s, 3H), 2.45 (s, 4H), 2.33–2.25 (m, 2H), 1.45–1.38 (m, 2H), 1.34–1.25 (m, 2H), 0.88 (t, J = 7.3 Hz, 3H). ^{13}C NMR (100 MHz, DMSO-d_6) δ 194.14, 187.40, 165.98, 153.08, 143.88, 143.34, 139.64, 132.46, 130.30, 129.90, 121.06, 118.36, 106.44, 60.10, 56.84, 56.10, 52.15, 41.30, 28.36, 19.99, 13.84. HR-MS (ESI):Calcd. $C_{29}H_{38}N_3O_5S_2$, $[M+H]^+$ m/z: 572.2253, found: 572.2258.

4.3.10. (E)-2-oxo-2-((4-(3-(3,4,5-trimethoxyphenyl)acryloyl)phenyl) amino)ethyl −4-(methylsulfonyl)piperazine-1-carbodithioate (12i)

Yellow solid; M.p.: 183–185 °C; Yield: 62%. ^{1}H NMR (400 MHz, DMSO-d_6) δ 10.70 (s, 1H), 8.18 (d, J = 8.8 Hz, 2H), 7.90 (d, J = 15.5 Hz, 1H), 7.79 (d, J = 8.8 Hz, 2H), 7.68 (d, J = 15.5 Hz, 1H), 7.23 (s, 2H), 4.35 (s, 2H), 4.32 (s, 2H), 4.13 (s, 2H), 3.87 (s, 6H), 3.72 (s, 3H), 3.29 (s, 4H), 2.95 (s, 3H). ^{13}C NMR (100 MHz, DMSO-d_6) δ 195.35, 187.42, 165.84, 153.08, 143.90, 143.31, 139.64, 132.47, 130.29, 129.93, 121.07, 118.36, 106.46, 60.11, 56.12, 44.87, 41.41, 34.40. HR-MS (ESI):Calcd. $C_{26}H_{32}N_3O_7S_3$, $[M+H]^+$ m/z: 594.1402, found: 594.1407.

4.3.11. (E)-2-oxo-2-((4-(3-(3,4,5-trimethoxyphenyl)acryloyl)phenyl) amino)ethyl- morpholine-4-carbodithioate (12j)

Yellow solid; M.p.: 176–178 °C; Yield: 60%. ^{1}H NMR (400 MHz, DMSO-d_6) δ 10.70 (s, 1H), 8.18 (d, J = 8.6 Hz, 2H), 7.90 (d, J = 15.5 Hz, 1H), 7.80 (d, J = 8.6 Hz, 2H), 7.69 (d, J = 15.5 Hz, 1H), 7.23 (s, 2H), 4.35 (s, 2H), 4.21 (s, 2H), 4.08–3.94 (m, 2H), 3.87 (s, 6H), 3.72 (s, 3H), 3.70 (s, 4H). ^{13}C NMR (100 MHz, DMSO-d_6) δ 194.90, 187.45, 165.96, 153.07, 143.91, 143.31, 139.61, 132.45, 130.29, 129.92, 121.06, 118.38, 106.41, 65.53, 60.11, 56.10, 55.63, 41.09. HR-MS (ESI):Calcd. $C_{25}H_{29}N_2O_6S_2$, $[M+H]^+$ m/z: 517.1467, found: 517.1469.

4.3.12. (E)-2-oxo-2-((4-(3-(3,4,5-trimethoxyphenyl)acryloyl)phenyl) amino)ethyl -thiomorpholine-4-carbodithioate 1,1-dioxide (12 k)

Yellow solid; M.p.: 179–181 °C; Yield: 74%. ^{1}H NMR (400 MHz, DMSO-d_6) δ 10.74 (s, 1H), 8.20 (d, J = 8.7 Hz, 2H), 7.91 (d, J = 15.5 Hz, 1H), 7.81 (d, J = 8.7 Hz, 2H), 7.70 (d, J = 15.5 Hz, 1H), 7.24 (s, 2H), 4.57 (s, 4H), 4.37 (s, 2H), 3.88 (s, 6H), 3.73 (s, 3H), 3.38 (s, 4H). ^{13}C NMR (100 MHz, DMSO-d_6) δ 197.10, 187.44, 165.62, 153.07, 143.91, 143.23, 139.64, 132.54, 130.29, 129.93, 121.06, 118.43, 106.44, 60.11, 56.10, 50.54, 42.24, 29.56. HR-MS (ESI):Calcd. $C_{25}H_{29}N_2O_7S_3$, $[M+H]^+$ m/z: 565.1137, found: 565.1139.

*4.3.13. (E)-2-oxo-2-((4-(3-(3,4,5-trimethoxyphenyl)acryloyl)phenyl) amino)ethyl piperidine-1-carbodithioate **(12l)***

Yellow solid; M.p.: 168–170 °C; Yield: 79%. ^{1}H NMR (400 MHz, DMSO-d_6) δ 10.67 (s, 1H), 8.18 (d, J = 8.8 Hz, 2H), 7.90 (d, J = 15.5 Hz, 1H), 7.80 (d, J = 8.8 Hz, 2H), 7.69 (d, J = 15.5 Hz, 1H), 7.23 (s, 2H), 4.31 (s, 2H), 4.21 (s, 2H), 3.94 (s, 2H), 3.87 (s, 6H), 3.72 (s, 3H), 1.70–1.54 (m, 6H). ^{13}C NMR (100 MHz, DMSO-d_6) δ 192.97, 187.45, 166.10, 153.09, 143.87, 143.34, 139.69, 132.47, 130.30, 129.89, 121.12, 118.39, 106.48, 60.11, 56.13, 52.58, 51.08, 41.39, 25.80, 25.13, 23.44. HR-MS (ESI):Calcd. $C_{26}H_{31}N_2O_5S_2$, $[M+H]^+$ m/z: 515.1674, found: 515.1679.

*4.3.14. (E)-2-oxo-2-((4-(3-(3,4,5-trimethoxyphenyl)acryloyl)phenyl) amino)ethylpyrrolidine-1-carbodithioate **(12m)***

Yellow solid; M.p.: 190–192 °C; Yield: 84%. ^{1}H NMR (400 MHz, DMSO-d_6) δ 10.65 (s, 1H), 8.18 (d, J = 8.8 Hz, 2H), 7.90 (d, J = 15.5 Hz, 1H), 7.79 (d, J = 8.8 Hz, 2H), 7.68 (d, J = 15.5 Hz, 1H), 7.23 (s, 2H), 4.31 (s, 2H), 3.87 (s, 6H), 3.77 (t, J = 6.9 Hz, 2H), 3.72 (s, 3H), 3.71–3.66 (m, 2H), 2.10–2.01 (m, 2H), 1.94 (dd, J = 13.4, 6.5 Hz, 2H). ^{13}C NMR (100 MHz, DMSO-d_6) δ 190.09, 187.45, 166.11, 153.09, 143.87, 143.32, 139.69, 132.47, 130.30, 129.89, 121.11, 118.39, 106.49, 60.12, 56.14, 55.21, 50.61, 40.85, 25.67, 23.78. HR-MS (ESI):Calcd. $C_{25}H_{29}N_2O_5S_2$, $[M+H]^+$ m/z: 501.1518, found: 501.1524.

4.4. Cell culture and MTT assay

MGC803 (human gastric cancer), PC3(human prostate cancer), and MCF7(human breast cancer) were cultured in an atmosphere containing 5% CO_2 at 37 °C, with RPMI-1640 medium with 10% fetal bovine serum, 100 U/ml penicillin and 0.1 mg/ml streptomycin.

Cells were seeded at a density of 5×10^3 per well in 96-well plates for 72 h. Then, 20 μL MTT solution was added to each well, and incubated for 4 h at 37 °C. 150 μL DMSO was added to each well to dissolve the formazan after removing the liquid, the absorbance was determined at 570 nm.

4.5. Clonogenicity assay

PC3 cells were seeded in a 6-well plate and incubated in 5% CO_2 at 37 °C for 24 h, then treated with the targeted compound **12d**. After 10 days, remove the culture medium, wash the cells twice with PBS, fix with 4% paraformaldehyde and stain with 0.1% crystal violet. The cells' image were captured, and the number of colonies were quantified by Image J software (National Institutes of Health).

4.6. Cell cycle distribution assay

PC3 cells were seeded in 6-well culture plate and treated with compound **12d** for 48 h. Then cells were harvested and fixed with 70% ethanol at 4 °C for 8 h. The fixed cells were washed and resuspended with PBS containing 10 mg/mL RNaseA and 50 mg/mL PI incubated for 25 min in dark. After that, samples were analyzed for DNA content with flow cytometry. (Becton, Dickinson and Company, NJ.)

4.7. Cell apoptosis assay

PC3 cells were seeded in 6-well culture plate and treated with compound **12d** for 48 h. Then cells were harvested and suspended in binding buffer containing Annexin V-FITC (0.5 mg/mL) and PI (0.5 mg/mL) and incubated for 25 min in dark. After that, samples were analyzed with flow cytometry (Becton, Dickinson and Company, NJ)

4.8. Migration assay

100 μL RPMI-1640 medium containing 1% fetal bovine serum, different concentrations of compound **12d** and 1x10^4 cells were added to each trans-well upper chamber. 500 μL medium with 20% fetal bovine serum was used as chemoattractant in the lower chamber. After 48 h incubation, both chambers were washed with PBS three times. Then stain the cells with crystal violet and analyze the image with image J software (National Institutes of Health).

4.9. Catalase specific activity

Human catalase activity of treated and untreated PC3 cells was detected using a catalase analysis kit (Beyotime Biotechnology, China). Briefly, working solution was heated in 37 °C 10 min previously, then add the treated and untreated PC3 cells lysate and determine the samples at 520 nm.

4.10. Measurement of loss of mitochondrial membrane potential (MMP, ΔΨ)

JC-1 probe was used to measure the loss of MMP. Cells were seeded at a density of 1.5×10^5 each well in 6-well plates, and treated with compound **12d** for 48 h. 2.5 μg/ml JC-1were added and incubated at 37 °C for 10 min. Then cells were analyzed with fluorescence microscope and flow cytometry after another two times wash.

4.11. Measurement of ROS

2,7-Dichlorodihydro fluorescent diacetate (DCFH-DA) was used to measure the levels of intracellular reactive oxygen species (ROS). Cells were seeded into a 6-well plate, and treated with compound **12d**. Following the treatment, cells were incubated with 20 mM DCFH-DA for 30 min at 37 °C in dark. Then cells were analyzed with fluorescence microscope after another two times wash.

4.12. Western blot analysis

Treated and untreated cells were harvested and lysed. Protein lysates were denatured and resolved by SDS-PAGE and transferred to nitrocellulose membrane. The membranes were incubated with appropriate antibodies at 4 °C for 8 h after blocking with 5% skimmed milk. After conjugated with secondary antibodies, the detection of proteins was carried out with an ECL kit.

4.13. Molecular docking

The Molecular Operating Environment software was used for docking studies. The X-ray crystal structure of the Catalase (CAT) was retrieved from the Protein Data Bank (PDB ID: 1DGG) and prepared using the default parameters. Hydrogen atoms and the partial charges for all atoms were added and water molecules were deleted. Energy-minimized was done to the CAT using Amber 10: EHT forcefield. With MOE-site Finder the CAT docking site was generated. Amber 10: EHT forcefield was also used for the 3D structures of compound building and energy-minimize. The London dG and Triangle Matcher placement method was used for docking. GBVI/WSA dG scoring function was used for conformation optimization to evaluate the final docking conformation. The docking results retain the top 30 in scoring.

4.14. Comet assay

PC3 cells were treated with different concentration of compound **12d** for 48 h. Then the cells were harvested and covered with comet slides. The slides were immersed in the lysis buffer for 2 h at 4 °C. After lyses, Comet slides were immersed in freshly and cold electrophoresis buffer for 25 min to equilibrate the slides. After equilibrating, electrophoresis was conducted at 25 V, 300 mA, for 30 min. Then the slides coated with drops of neutralization buffer for 5 min, repeated three times. The slides were stained with 1.0 μg/ml DAPI, and observed with

a fluorescent microscope.

4.15. Statistical analysis

Data from three independent experiments are presented as mean ± SD. IC_{50} values and Student's *t*-tests were calculated by SPSS version 10.0 (SPSS, Inc., Chicago, IL, USA). ** and *** respectively represent $p < 0.01$ and $p < 0.001$.

Acknowledgment

This work was supported by the National Natural Sciences Foundations of China (No. 81703541 and 81673322), and project funded by China Postdoctoral Science Foundation. This work was supported by MEDCHEMEXPRESS. Thanks to MCE Award for Scientists Promoting Biology and Medicine Research.

Appendix A. Supplementary material

Supplementary data to this article can be found online at https://doi.org/10.1016/j.bioorg.2019.01.023.

References

[1] P. Singh, A. Anand, V. Kumar, Recent developments in biological activities of chalcones: a mini review, Eur. J. Med. Chem. 85 (2014) 758–777.
[2] D.-J. Fu, S.-Y. Zhang, Y.-C. Liu, X.-X. Yue, J.-J. Liu, J. Song, R.-H. Zhao, F. Li, H.-H. Sun, Y.-B. Zhang, H.-M. Liu, Design, synthesis and antiproliferative activity studies of 1,2,3-triazole-chalcones, MedChemComm. 7 (2016) 1664–1671.
[3] S.-Y. Zhang, D.-J. Fu, X.-X. Yue, Y.-C. Liu, J. Song, H.-H. Sun, H.-M. Liu, Y.-B. Zhang, Design, synthesis and structure-activity relationships of novel chalcone-1,2,3-triazole-azole derivates as antiproliferative agents, Molecules 21 (2016) 653.
[4] L. Li, S. Jiang, X. Li, Y. Liu, J. Su, J. Chen, Recent advances in trimethoxyphenyl (TMP) based tubulin inhibitors targeting the colchicine binding site, Eur. J. Med. Chem. 151 (2018) 482–494.
[5] D. Raffa, B. Maggio, M.V. Raimondi, F. Plescia, G. Daidone, Recent discoveries of anticancer flavonoids, Eur. J. Med. Chem. 142 (2017) 213–228.
[6] F.F. Ahmed, A.A. Abd El-Hafeez, S.H. Abbas, D. Abdelhamid, M. Abdel-Aziz, New 1,2,4-triazole-Chalcone hybrids induce Caspase-3 dependent apoptosis in A549 human lung adenocarcinoma cells, Eur. J. Med. Chem. 151 (2018) 705–722.
[7] Y. Wang, A. Hedblom, S.K. Koerner, M. Li, F.E. Jernigan, B. Wegiel, L. Sun, Novel synthetic chalcones induce apoptosis in the A549 non-small cell lung cancer cells harboring a KRAS mutation, Bioorg. Med. Chem. Lett. 26 (2016) 5703–5706.
[8] Q. Li, P. Zou, J. Sun, L. Chen, O2-(2,4-dinitrophenyl)diazeniumdiolates derivatives: design, synthesis, cytotoxic evaluation and reversing MDR in MCF-7/ADR cells, Eur. J. Med. Chem. 143 (2018) 732–744.
[9] M. Wang, S. Xu, C. Wu, X. Liu, H. Tao, Y. Huang, Y. Liu, P. Zheng, W. Zhu, Design, synthesis and activity of novel sorafenib analogues bearing chalcone unit, Bioorg. Med. Chem. Lett. 26 (2016) 5450–5454.
[10] K. Nepali, S. Sharma, M. Sharma, P.M.S. Bedi, K.L. Dhar, Rational approaches, design strategies, structure activity relationship and mechanistic insights for anticancer hybrids, Eur. J. Med. Chem. 77 (2014) 422–487.
[11] C.R. Yang, B. Peng, S.L. Cao, T.T. Ren, W. Jiang, F.C. Wang, Y.S. Li, G. Wang, Z. Li, S. Xu, Synthesis, cytotoxic evaluation and target identification of thieno[2,3-d] pyrimidine derivatives with a dithiocarbamate side chain at C2 position, Eur. J. Med. Chem. 154 (2018) 324.
[12] S. Laskar, L. Sánchezsánchez, S.M. Flores, H. Lópezmuñoz, M.L. Escobarsánchez, M. Lópezortiz, M. Hernándezrodríguez, I. Regla, Identification of (1S,4S)-2,5-diazabicyclo[2.2.1]heptane-dithiocarbamate-nitrostyrene hybrid as potent antiproliferative and apoptotic inducing agent against cervical cancer cell lines, Eur. J. Med. Chem. (2018) 621–635.
[13] D.-J. Fu, L. Zhang, J. Song, R.-W. Mao, R.-H. Zhao, Y.-C. Liu, Y.-H. Hou, J.-H. Li, J.-J. Yang, C.-Y. Jin, P. Li, X.-L. Zi, H.-M. Liu, S.-Y. Zhang, Y.-B. Zhang, Design and synthesis of formononetin-dithiocarbamate hybrids that inhibit growth and migration of PC-3 cells via MAPK/Wnt signaling pathways, Eur. J. Med. Chem. 127 (2017) 87–99.
[14] R.-D. Li, H.-L. Wang, Y.-B. Li, Z.-Q. Wang, X. Wang, Y.-T. Wang, Z.-M. Ge, R.-T. Li, Discovery and optimization of novel dual dithiocarbamates as potent anticancer agents, Eur. J. Med. Chem. 93 (2015) 381–391.
[15] M.D. Altıntop, B. Sever, G. Akalın Çiftçi, K. Kucukoglu, A. Özdemir, S.S. Soleimani, H. Nadaroglu, Z.A. Kaplancıklı, Synthesis and evaluation of new benzodioxole-based dithiocarbamate derivatives as potential anticancer agents and hCA-I and hCA-II inhibitors, Eur. J. Med. Chem. 125 (2017) 190–196.
[16] S.-L. Cao, Y. Wang, L. Zhu, J. Liao, Y.-W. Guo, L.-L. Chen, H.-Q. Liu, X. Xu, Synthesis and cytotoxic activity of N-((2-methyl-4(3H)-quinazolinon-6-yl)methyl)dithiocarbamates, Eur. J. Med. Chem. 45 (2010) 3850–3857.
[17] D.J. Fu, J. Song, Y.H. Hou, R.H. Zhao, J.H. Li, R.W. Mao, J.J. Yang, P. Li, X.L. Zi, Z.H. Li, Discovery of 5,6-diaryl-1,2,4-triazines hybrids as potential apoptosis inducers, Eur. J. Med. Chem. 138 (2017) 1076–1088.
[18] M. Juhaszova, D.B. Zorov, S.-H. Kim, S. Pepe, Q. Fu, K.W. Fishbein, B.D. Ziman, S. Wang, K. Ytrehus, C.L. Antos, E.N. Olson, S.J. Sollott, Glycogen synthase kinase-3β mediates convergence of protection signaling to inhibit the mitochondrial permeability transition pore, J. Clin. Invest. 113 (2004) 1535–1549.
[19] D.J. Fu, Y.C. Liu, J.J. Yang, J. Zhang, C.D. Xiong, Z.S. Cao, X.X. Yin, W. Wei, Y.B. Zhang, Design and synthesis of sulfonamide-1,2,3-triazole derivatives bearing a dithiocarbamate moiety as antiproliferative agents, J. Chem. Res. 41 (2017) 523–525.
[20] H.M. Liu, Y.B. Zhang, Y.C. Liu, R.H. Zhao, J. Song, D.J. Fu, Synthesis of novel antiproliferative 1,2,3-triazole hybrids using the molecular hybridisation approach, J. Chem. Res. 40 (2016) 674–677.
[21] D.J. Fu, Y.H. Hou, S.Y. Zhang, Y.B. Zhang, Efficient click reaction towards novel sulfonamide hybrids by molecular hybridization strategy as antiproliferative agents, J. Chem. Sci. 130 (2018) 6.
[22] D.J. Fu, J.F. Liu, R.H. Zhao, J.H. Li, S.Y. Zhang, Y.B. Zhang, Design and antiproliferative evaluation of novel sulfanilamide derivatives as potential tubulin polymerization inhibitors, Molecules 22 (2017) 1470.
[23] D.J. Fu, S.Y. Zhang, Y.C. Liu, L. Zhang, J.J. Liu, J. Song, R.H. Zhao, F. Li, H.H. Sun, H.M. Liu, Design, synthesis and antiproliferative activity studies of novel dithiocarbamate-chalcone derivates, Bioorg. Med. Chem. Lett. 26 (2016) 3918–3922.
[24] D.J. Fu, R.H. Zhao, J.H. Li, J.J. Yang, R.W. Mao, B.W. Wu, P. Li, X.L. Zi, Q.Q. Zhang, H.J. Cai, Molecular diversity of phenothiazines: design and synthesis of phenothiazine-dithiocarbamate hybrids as potential cell cycle blockers, Mol. Divers. 21 (2017) 933–942.
[25] D.J. Fu, L. Fu, Y.C. Liu, J.W. Wang, Y.Q. Wang, B.K. Han, X.R. Li, C. Zhang, F. Li, J. Song, Structure-activity relationship studies of β-lactam-azide analogues as orally active antitumor agents targeting the tubulin colchicine site, Sci. Rep. 7 (2017) 12788.
[26] D.-J. Fu, J.-J. Yang, P. Li, Y.-H. Hou, S.-N. Huang, M.A. Tippin, V. Pham, L. Song, X. Zi, W.-L. Xue, L.-R. Zhang, S.-Y. Zhang, Bioactive heterocycles containing a 3,4,5-trimethoxyphenyl fragment exerting potent antiproliferative activity through microtubule destabilization, Eur. J. Med. Chem. 157 (2018) 50–61.
[27] J.W. Harper, G.R. Adami, N. Wei, K. Keyomarsi, S.J. Elledge, The p21 Cdk-interacting protein Cip1 is a potent inhibitor of G1 cyclin-dependent kinases, Cell 75 (1993) 805.
[28] J. Yang, R.A. Weinberg, Epithelial-mesenchymal transition: at the crossroads of development and tumor metastasis, Dev. Cell 14 (2008) 818–829.
[29] R.A. Whipple, M.A. Matrone, E.H. Cho, E.M. Balzer, M.I. Vitolo, J.R. Yoon, O.B. Ioffe, K.C. Tuttle, J. Yang, S.S. Martin, Epithelial-to-mesenchymal transition promotes tubulin detyrosination and microtentacles that enhance endothelial engagement, Cancer Res. 70 (2010) 8127–8137.
[30] X. Qin, L. Fang, F. Chen, S. Gou, Conjugation of platinum(IV) complexes with chlorambucil to overcome cisplatin resistance via a "joint action" mode toward DNA, Eur. J. Med. Chem. 137 (2017) 167–175.
[31] Z.-Z. Wei, Q.-P. Qin, T. Meng, C.-X. Deng, H. Liang, Z.-F. Chen, 5-Bromo-oxoisoaporphine platinum(II) complexes exhibit tumor cell cytotoxcicity via inhibition of telomerase activity and disruption of c-myc G-quadruplex DNA and mitochondrial functions, Eur. J. Med. Chem. 145 (2018) 360–369.
[32] D. Wan, B. Tang, Y.-J. Wang, B.-H. Guo, H. Yin, Q.-Y. Yi, Y.-J. Liu, Synthesis and anticancer properties of ruthenium (II) complexes as potent apoptosis inducers through mitochondrial disruption, Eur. J. Med. Chem. 139 (2017) 180–190.
[33] P.R. Kamath, D. Sunil, A.A. Ajees, K.S.R. Pai, S. Biswas, N′-((2-(6-bromo-2-oxo-2H-chromen-3-yl)-1H-indol-3-yl)methylene)benzohydrazide as a probable Bcl-2/Bcl-xL inhibitor with apoptotic and anti-metastatic potential, Eur. J. Med. Chem. 120 (2016) 134–147.
[34] M. Zhou, S. Ji, Z. Wu, Y. Li, W. Zheng, H. Zhou, T. Chen, Synthesis of selenazolopyridine derivatives with capability to induce apoptosis in human breast carcinoma MCF-7 cells through scavenge of intracellular ROS, Eur. J. Med. Chem. 96 (2015) 92–97.
[35] M. Nishikawa, M. Hashida, Y. Takakura, Catalase delivery for inhibiting ROS-mediated tissue injury and tumor metastasis, Adv. Drug. Deliver. Rev. 61 (2009) 319–326.
[36] C.D. Putnam, A.S. Arvai, Y. Bourne, J.A. Tainer, Active and inhibited human catalase structures: ligand and NADPH binding and catalytic mechanism11Edited by R. Huber, J. Mol. Biol. 296 (2000) 295–309.